Talanta 190 (2018) 70–77

Contents lists available at ScienceDirect

Talanta

journal homepage: www.elsevier.com/locate/talanta

Layer-by-layer chitosan-decorated pristine graphene on screen-printed electrodes by one-step electrodeposition for non-enzymatic hydrogen peroxide sensor

Qin Zhu[a], Bo Liang[a,*], Yu Cai[a], Qingpeng Cao[a], Tingting Tu[a], Bobo Huang[a], Lu Fang[b], Xuesong Ye[a,*]

[a] Biosensor National Special Laboratory, Key Laboratory of Biomedical Engineering of Ministry of Education, College of Biomedical Engineering and Instrument Science, Innovation Center for Minimally Invasive Technique and Device, Zhejiang University, Hangzhou 310027, PR China
[b] College of Life Information Science and Instrument Engineering, Hangzhou Dianzi University, Hangzhou 310018, PR China

ARTICLE INFO

Keywords:
Pristine graphene
Chitosan
Co-electrodeposition
Hydrogen peroxide biosensor
Screen-printed electrodes

ABSTRACT

Layer-by-layer chitosan-decorated pristine graphene on screen-printed electrodes was achieved by one-step electrodeposition method and an enzyme-free hydrogen peroxide electrochemical biosensor was fabricated for its application. Negatively charged pristine graphene absorbed with positively charged chitosan by electrostatic interactions was electrodeposited on the electrodes. The successful immobilization of pristine graphene was confirmed by scanning electron microscopy (SEM), Fourier transform infrared spectroscopy (FTIR), Raman spectroscopy, X-ray photoelectron spectroscopy (XPS) and electrochemical characterizations. The graphene-chitosan volume ratio and cyclic voltammetry scan cycles during the electrodeposition process were optimized. The resulting hydrogen peroxide biosensors showed a 178 times improved sensitivity and exhibited two wide linear detection ranges from 20 μM to 20 mM and from 20 mM to 60 mM. The biosensors also showed a good reproducibility, stability, selectivity and could be used in real samples detection. The superior electrochemical performance of graphene-chitosan was attributed to the preservation of excellent properties of pristine graphene, and the formation of layer-by-layer structure with high surface area. The proposed strategy of direct immobilization of pristine graphene can be extended for the immobilization of other nanomaterials and biomolecules.

1. Introduction

Graphene, one-atom-thick two-dimensional honeycomb crystal lattice of carbon atoms with an sp^2 hybridized structure [1], has been widely used in the fields of electrochemistry, biosensors, fuel cell, supercapacitors and so on, due to its ease of functionalization, fast electron transfer capabilities, large specific surface area, excellent electrical and thermal conductivities. Pristine graphene possesses uniform pi-electron distribution and few defect, showing high conductivity, excellent electron transfer and strong adsorption capacity, thus proved itself a good catalyst support [2]. However, it is difficult to uniformly and effectively immobilize graphene because graphene sheets tend to restack together due to van der Waals [3–5] and strong π-π interaction, thus forming a densely packed layered structure, accompanied by the loss of many unique properties.

The most common technique to immobilize graphene is via the oxidation of graphite to yield graphene oxide (GO) suspension, followed by the reduction of GO to obtain reduced graphene oxide (RGO) through chemical [6], thermal [7] or electrochemical [8] reduction method, and the immobilization of RGO was achieved at the same time. Nevertheless, the unique properties of pristine graphene could not fully restore after the reduction due to the retention of oxidation in RGO [9], although intrinsic defect and electrical insulation of GO have been improved by the reduction to some extent [10]. The conductivity of reduced GO monolayers is approximately 3 orders of magnitude lower than pristine graphene [10]. Hence the effective immobilization method of pristine graphene with preservation of its intrinsic extraordinary conductivity is of great demand.

Chitosan (CS) is a polysaccharide widely used as the matrix for entrapment of biomolecules and nanomaterials due to its excellent film forming ability [11], good adhesion, nontoxicity and biocompatibility. When protonated in slightly acidic solution and positively charged with

* Corresponding authors.
E-mail addresses: boliang1986@zju.edu.cn (B. Liang), yexuesong@zju.edu.cn (X. Ye).

https://doi.org/10.1016/j.talanta.2018.07.038
Received 13 May 2018; Received in revised form 9 July 2018; Accepted 11 July 2018
Available online 27 July 2018
0039-9140/

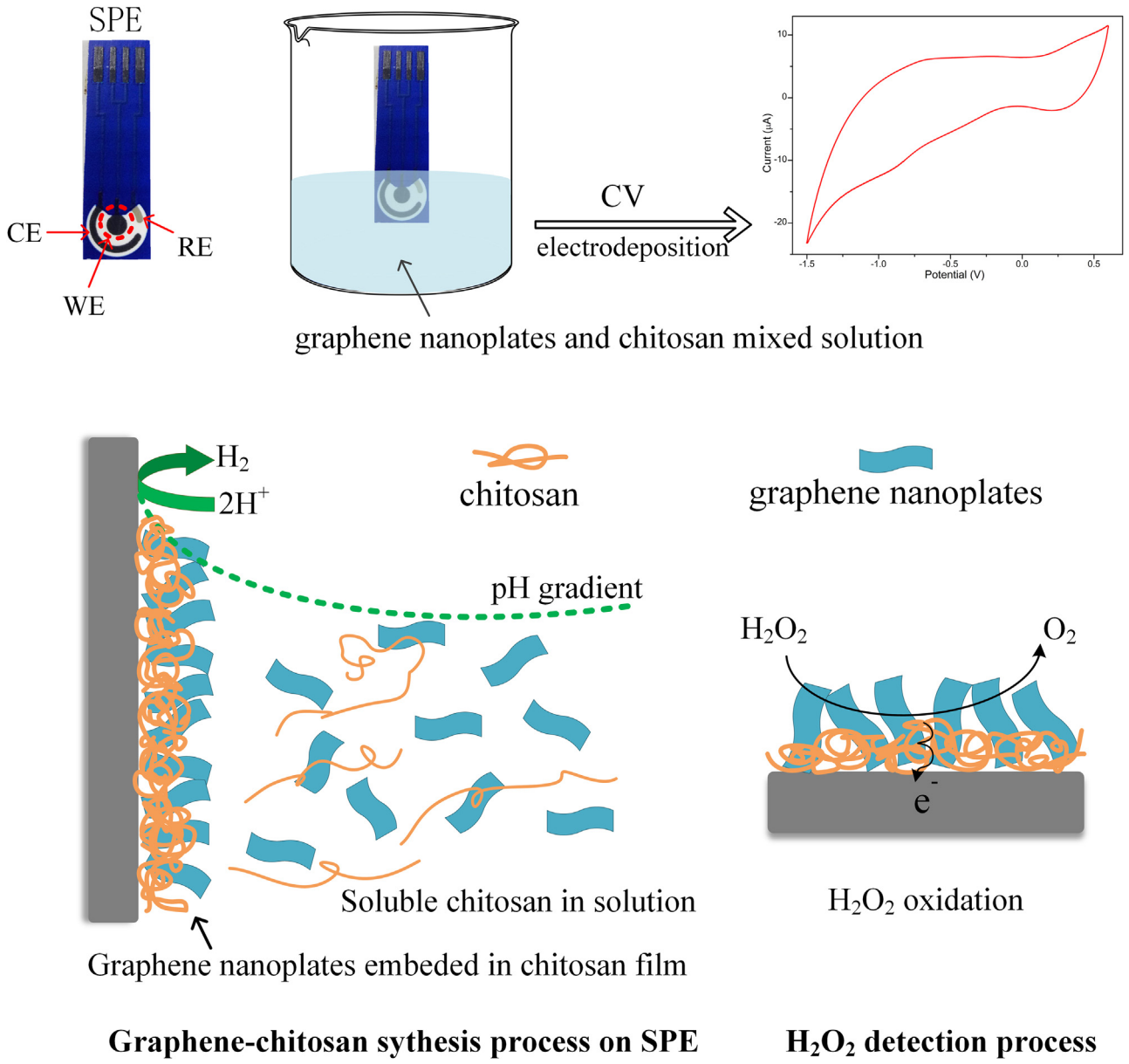

Scheme 1. Schematic illustration of pristine graphene immobilization procedure via one-step cyclic voltammetry electrodeposition method.

-$NH3^+$ groups, chitosan can adhere to negatively charged materials [12] to prevent the aggregation [13] and immobilize them onto the surface of the electrodes. Therefore, a variety of researches [14–16] have integrated chitosan with such materials for the fabrication of electrochemical biosensors to improve biosensor characteristics. However, in these applications, chitosan-containing mixed solution was casting or dropping onto the electrode surfaces. Thus, the thickness of the hybrid film was hardly controllable, leading to a loss of active surface area [17], and the reproducibility of the sensors could not be guaranteed. The electrodeposition method for sensor fabrication has been proved to be an effective solution for such problem as reported previously [18,19].

Compared with traditional fabrication techniques, electrodeposition method has the advantage of convenient operation, reproducibility and controllable thickness of obtained films by altering electrochemical experiment conditions. When the pH does not exceed pK_a of 6.3, many amino groups of CS are protonated, and CS is soluble. Successful electrodeposition of the CS sol-gel film has been achieved through H^+ consuming at the cathode, thus locally pH gradient established and the solubility of CS decreased, eventually resulting in a reproducible and stable CS film on the electrodes [18,20]. Other materials such as carbon nanotubes [21] and Pt nanoparticles [22] can also be immobilized onto the electrode along with CS films during the electrodeposition at the same time. However, studies about one-step co-electrodeposition of pristine graphene nanoplates and chitosan by CV method has not been explored thus far.

Screen-printed electrodes have been extensively used for biosensors owing to its properties, such as low cost, reproducibility, portability and mass production [23–25]. Here, a low-cost, facile and effective method for the direct immobilization of pristine graphene nanoplates on screen-printed electrodes has been proposed for the first time via one-step co-electrodeposition in the graphene and chitosan mixed solution, as depicted in Scheme 1. In order to explore the electrochemical sensor applications of the graphene-chitosan, enzyme-free hydrogen peroxide biosensor was fabricated. The presence of pristine graphene nanoplates provide the excellent catalytic activity for hydrogen peroxide, and positively charged chitosan acts as effective cross-linkage to immobilize negatively charged pristine graphene nanoplates via electrostatic

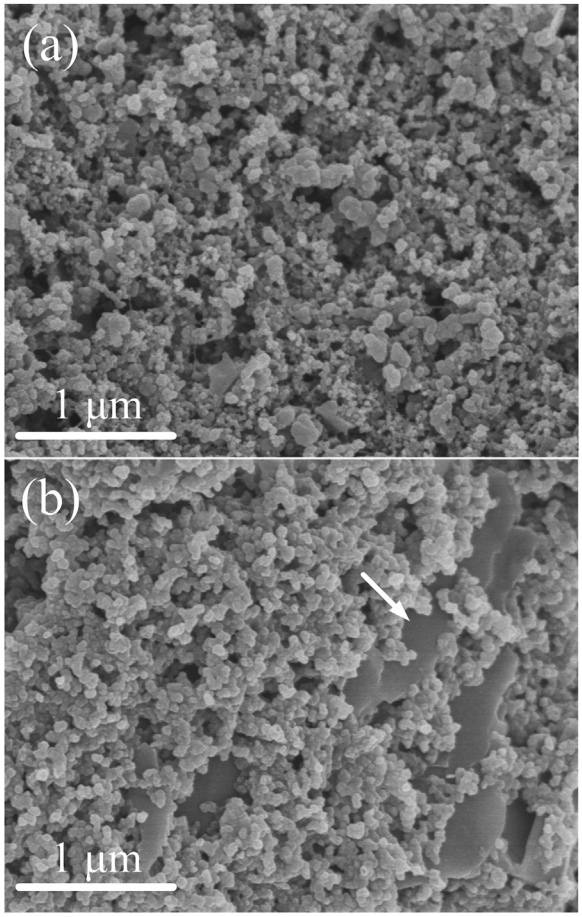

Fig. 1. SEM images of blank SPE (a) and graphene-chitosan/SPE (b).

interactions. Co-electrodeposition conditions of graphene-chitosan hybrid film have been optimized to evaluate their influence on the performance of the electrodes. The resulting graphene-chitosan demonstrates excellent catalysis performance towards H_2O_2 with a wide linear range and a low detection limit.

2. Experimental

2.1. Apparatus

The morphologies and structures of the modified screen-printed electrodes were characterized using a field emission scanning electron microscope (FESEM, Hitachi SU8010). The Raman spectra were measured using a LabRAM HR Evolution spectrometer (Horiba Jobin Yvon) with an excitation wavelength of 532 nm in 400–3000 cm^{-1} region at room temperature. FTIR was obtained using a Nicolet iS 10 FTIR Infrared Microscopy (Thermo Fisher Scientific, U.S.A) with an wavelength of 350–7800 cm^{-1}. The XPS spectra of the electrodes were obtained by VG ESCALAB MARK II spectrometer with the energy resolution at 0.8 eV. All electrochemical experiments were performed using an electrochemical workstation (μAutolab III, Metrohm, Switzerland) on a typical three-electrode system. Screen-printed electrodes (SPEs) were composed of an Ag/AgCl pseudo-reference electrode, a carbon paste counter electrode, and a carbon paste electrode as the working electrode (Ø = 3 mm). The distance between the center of working electrode and the inner edge of reference electrode or counter electrode is 3 mm.

2.2. Reagents

Pet ink 9000 series (9045, deep blue) and Jelcon CH-8 (MOD 2) carbon ink were obtained from Jujo Chemical Co., Ltd. (Tokyo, Japan). Silver paste (DD-1) was purchase from Guangzhou Saidi Technology Development Co., Ltd. Silver chloride paste (CNC-01) was obtained from Yingman Nano Technology Jiangsu Co., Ltd. Pristine graphene nanoplates (XF022-1, lateral size 1–3 μm, thickness 1–5 nm, conductivity 500–1000 S/cm) were purchased from Nanjing XFNANO Materials Tech Co. Ltd. (Nanjing, China). N-Methyl pyrrolidone (NMP) were obtained from Aladdin Ltd. (Shanghai, China). Chitosan, acetic acid and hydrogen peroxide 30% aqueous solution were obtained from Sinopharm Chemical Reagent Co., Ltd. Bovine serum was purchased from Hangzhou Qizhenhu Bioscience Co., Ltd. All chemicals are of analytical grade. Deionized-ultrafiltered (18 MΩ/cm) water was used for rinsing and the solvent.

2.3. Preparation of graphene-chitosan mixed solution

20 mg graphene nanoplates were dispersed in 4 mL N-Methyl pyrrolidone (NMP) with utra-sonication for 30 min. After centrifugation at 1000 rmp for 4 min, the supernatant was obtained. 1% chitosan solution was prepared by dissolving 1.0 g chitosan in 100 mL 1% acetic acid solution with stirring at 80 °C for 30 min 2 mL graphene nanoplates dispersion and four different volumes of chitosan solution were mixed for subsequent electrochemical experiments.

2.4. One-step synthesis of graphene-chitosan/SPE

Prior to the electrode modification, the screen-printed electrodes were treated by cyclic voltammetry (CV) with potential window from − 0.4–0.6 V at a scan rate of 50 mV/s in 1.0 M sulfuric acid (H_2SO_4) for 10 cycles and rinsed with deionized ultrafiltered water. Afterwards graphene-chitosan hybrid film was electrodeposited on the screen-printed electrodes with potential window from − 1.5–0.6 V at a scan rate of 50 mV/s in the graphene-chitosan mixed solution and denoted as graphene-CS/SPE. The whole process of graphene-chitosan/SPE fabrication was described in Scheme 1.

2.5. Optimization of the fabrication conditions for graphene-chitosan/SPE

Different graphene-chitosan ratio and several CV cycles were used to evaluate their influence on the performance of the electrodes and the optimal fabrication conditions for graphene-chitosan was found. For comparison, graphene nanoplates dispersion only and chitosan solution only were also prepared to be electrodeposited on SPE, denoted as graphene/SPE and CS/SPE respectively, and applied in the subsequent experiments.

2.6. Enzyme-free determination of hydrogen peroxide

Enzyme-free determination of hydrogen peroxide was carried out by performing chronoamperometry experiments in a 0.01 M phosphate-buffered saline (PBS) solution (pH 7.0) at room temperature unless otherwise specified. After an initial background stabilization period of 600 s, the amperometric experiments were performed by dropping 20 μL 1 M hydrogen peroxide solution into 25 mL PBS every 50 s.

3. Results and discussion

3.1. Characterizations of graphene-chitosan

Fig. 1 illustrates the SEM images of bare SPE and graphene-CS/SPE. Fig. 1b confirms the surface modification of graphene and chitosan on SPE, revealing the typical morphology of pristine graphene nanoplates and uniform chitosan coated surface morphology, similar to previous

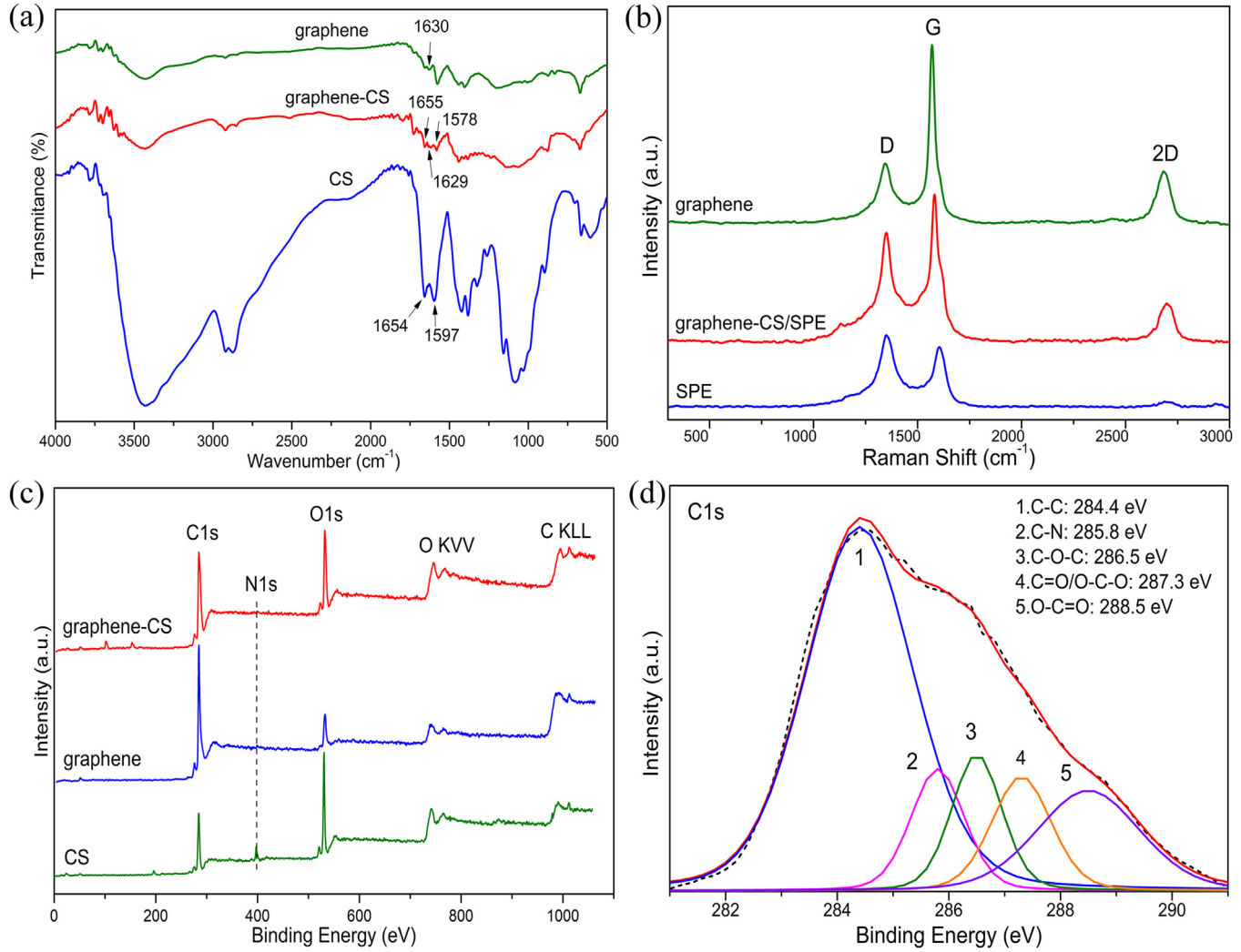

Fig. 2. (a) FTIR spectra of chitosan, graphene and as-prepared graphene-chitosan. (b) Raman spectra of bare SPE, graphene and as-prepared graphene-chitosan/SPE. (c) XPS full scan spectra of chitosan, graphene and as-prepared graphene-chitosan/SPE. (d) XPS C1s spectrum of as-prepared graphene-chitosan.

reports [15,19,20]. As identified with the white arrow in Fig. 1b, the co-electrodeposited graphene nanoplates are embedded in chitosan and layer-by-layer structure formed. CS is protonated in acetic acid and positively charged with $-NH_3^+$ groups in the solution. When mixed with CS solution, negatively charged graphene nanoplates interacted with positively charged CS due to electrostatic attractions and co-electrodeposited onto SPE. In contrast, SEM image of the blank screen-printed electrodes as shown in Fig. 1a reveals that the electrode was merely typical morphology assembled by graphite particles of different sizes. These observations indicate that the direct immobilization of pristine graphene on SPE could be fulfilled through one-step electrodeposition in the presence of chitosan.

The successful synthesis of graphene-chitosan was also validated by FTIR spectroscopy, identifying the functional groups and structural changes. Fig. 2a displays the FTIR spectra of pristine graphene nanoplates, chitosan and graphene-CS hybrid film. For pristine graphene nanoplates spectrum, the peak centered at 1630 cm^{-1} is assigned to C=C bonds [26], corresponding to skeletal vibrations of unoxidized graphite domains [27]. Two distinct peaks centered at 1654 cm^{-1} and 1597 cm^{-1} are observed at chitosan spectrum, attributed to the C=O stretching vibration of -NHCO- and the N-H bending vibrations of $-NH_2$, respectively [28]. The graphene-CS spectrum clearly demonstrates a combination of characteristic peaks corresponding to both graphene and chitosan, including the peak centered at 1655 cm^{-1} due to the C=O stretching vibration from chitosan, and the peak located at 1629 cm^{-1} owing to unoxidized graphitic skeletal vibrations from graphene [27]. The peak centered at 1597 cm^{-1} in the spectrum of chitosan shifted to 1578 cm^{-1} in the graphene-CS spectrum, suggesting the interactions newly formed between graphene and chitosan. The above results clearly indicate that graphene and chitosan have both functionalized on the electrodes.

The quality of the electrodeposited graphene-chitosan hybrid film was determined by Raman spectra analysis. Fig. 2b demonstrates the Raman spectra for SPE, graphene and as-prepared graphene-CS/SPE. Pristine graphene nanoplates shows the prominent peaks for D band (1345 cm^{-1}), G band (1569 cm^{-1}) and 2D band (2681 cm^{-1}). The G band corresponds to the ordered in-plane sp^2 bonded carbon vibration, while D band from the first-order scattering by zone-boundary phonons is related to sp^3-hybridized carbon, indicating defects or disordered structures [29]. The obtained graphene-CS/SPE exhibited a similar Raman spectrum as graphene nanoplates with D band at 1349 cm^{-1}, G band shifted to 1581 cm^{-1} and 2D band shifted to 2697 cm^{-1}, suggesting that the main structure of graphene nanoplates maintained in the hybrid film. However, the increased Raman intensity ratio (I_D/I_G) of graphene-CS indicates that changes in the hybridized carbon from sp^2 to sp^3 has already occurred as a consequence of coupling between pristine graphene nanoplates and chitosan via electrostatic interactions. This also may result from the formation of edge defects in the pristine

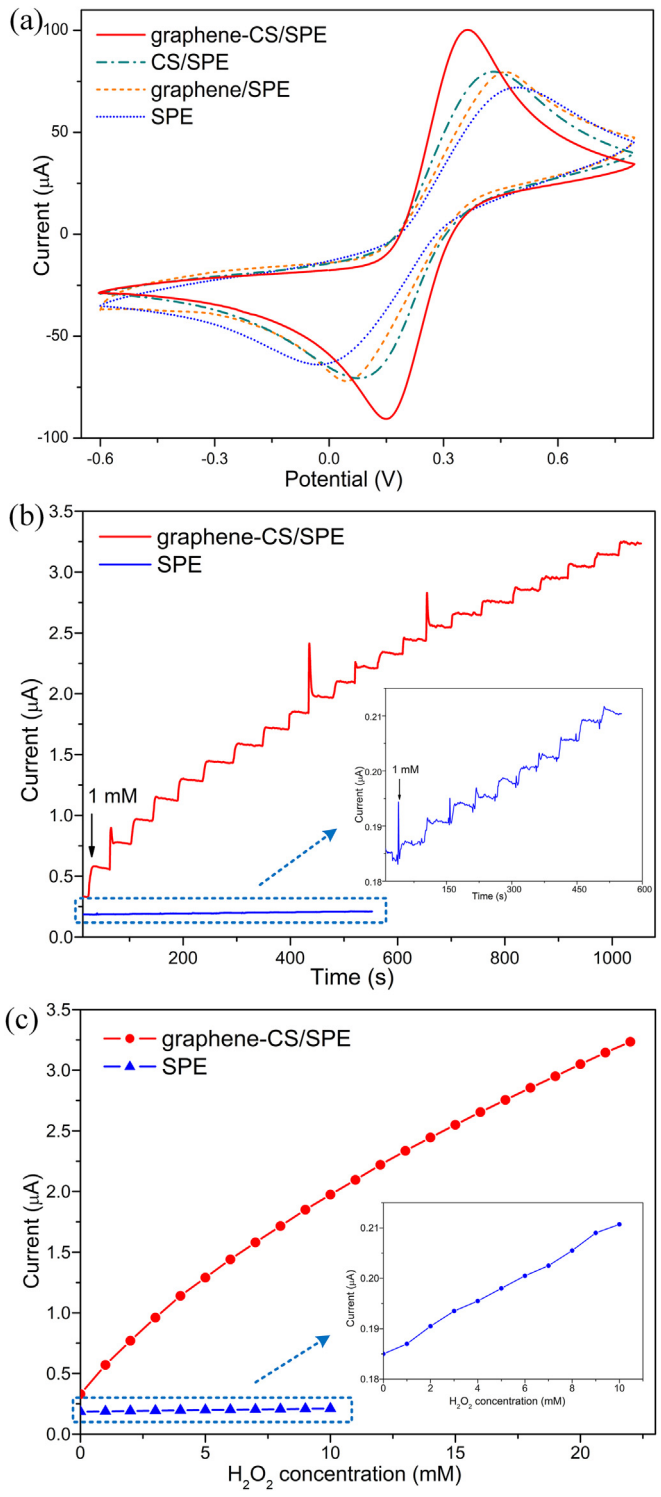

Fig. 3. (a) Cyclic voltammograms of 10 mM $[Fe(CN)_6]^{3-/4-}$ in 0.1 M KCl on bare SPE (in blue, shot dot), graphene/SPE (in orange, short dash), chitosan/SPE (in green, dash dot) and graphene-CS/SPE (in red, solid). The initial potential is 0 V and potential window is from − 0.6–0.8 V for all the scans. Scan rate: 50 mV/s. (b) Typical current-time response for successive addition of H_2O_2 for bare SPE (in blue) and graphene-CS/SPE (in red) at an applied potential of 0.6 V in 0.01 M PBS with stirring. The inset is the magnification of current response of bare SPE. (c) Calibration curves for H_2O_2 concentration determination at bare SPE (in blue) and graphene-CS/SPE (in red). The inset is the magnification of the calibration curve of bare SPE. (For interpretation of the references to color in this figure legend, the reader is referred to the web version of this article.).

graphene nanoplates during as-prepared dispersion and electrodeposition process. Full Raman spectra analysis results are shown in Table S1.

XPS analysis was broadly employed to explore the surface chemistry information such as identification of elements and analysis of chemical state. The C/O molar ratio of graphene, chitosan and graphene-CS calculated from the relative peak areas, was found to be 1:0.14, 1:0.45, 1:0.28 respectively, as shown in the full-scan XPS spectrum (Fig. 2c), confirming the successful combination of graphene and chitosan. In addition, the C/O molar ratio of bare SPE calculated from its full scan spectrum (Fig. S1) was determined to be 1:0.23 and an obvious peak of F1s existed which disappeared in graphene-CS/SPE, suggesting that a modification layer have been indeed synthetized on the SPE. The C1s spectrum of graphene-chitosan shown in Fig. 2d was deconvoluted into five Lorentzian-Gaussian peaks of 20:80 ratio, with the binding energy located at 284.4, 285.8, 286.5, 287.3 and 288.5 eV, assigned to C-C, C-N, C-O-C, C=O/O-C-O and O-C=O, respectively [30–32]. The C-N chemical bonds at 285.8 eV confirms the strong interactions between carbon and nitrogen bonds, attributed to chitosan (Fig. S2), suggesting the successful electrodeposition of chitosan. For pristine graphene nanoplates, the C1s core level spectrum (Fig. S3) displayed the peak at 284.5 eV, corresponding to the sp^2-hybridized graphitic carbon atoms arranged in the conjugated honeycomb lattice [33]. This peak is also dominant in graphene-CS with a slight shift of 0.1 eV, indicating that the majority of the carbon atoms remained the structures as in the pristine graphene nanoplates and a slight combination with chitosan. The relative area of the O-C=O peak increased to some extent after co-electrodeposition, indicating that the edge of pristine graphene nanoplates was carboxylated to some degree and could provide active sites for subsequent modification, consistent with the analysis results of Raman spectra. The presence of chitosan and graphene on the modified electrodes was clearly confirmed by the above analysis results, suggesting that the successful immobilization of pristine graphene nanoplates was achieved by one step electrodeposition method in the presence of chitosan.

3.2. Electrochemical behaviors of graphene-chitosan/SPE

CS is protonated and positively charged in 1% acetic acid. During the electrodeposition growth procedure as shown in Fig. S4, local pH gradient established and solubility of CS decreased, resulting in a reproducible and stable CS film on the electrodes. Fig. S4 demonstrates the fabrication curves of the modified electrodes through cyclic voltammetry method. Fig. S4 shows the cyclic voltammograms of SPEs in graphene-chitosan mixed solution (2 mL graphene and 1.5 mL 1% chitosan), 1% chitosan solution and as-prepared graphene nanoplates dispersion at a scan rate of 50 mV/s. No peaks are observed for graphene and the background current for graphene is quite small, indicating that graphene alone could be hardly electrodeposited on the electrodes. While a reduction peak at around − 0.80 V appears on other curves, indicating the formation of chitosan film. At the applied potential, H^+ in the solution is reduced to H_2, leading to an increased pH value near the electrode surface. When the pH exceeds p*K*a of 6.3, chitosan becomes insoluble and chitosan film forms. Moreover, the background current of graphene-CS is much higher than that of graphene, ascribed to the presence of chitosan, indicating that the addition of chitosan remarkably improves the adsorption and entrapment of the graphene nanoplates upon the electrode. The background current of graphene-chitosan is also higher than that of chitosan only, showing that the addition of graphene enhances the electroactivity of mixed solution. All in all, the synergistic effect of graphene and chitosan greatly promotes the electrodeposition of the graphene-chitosan film.

The electrochemical behaviors of the graphene-CS/SPE was investigated by cyclic voltammetry (CV) in 10 mM $[Fe(CN)_6]^{3-/4-}$ with 0.1 M KCl, as shown in Fig. 3a. For graphene-CS/SPE (in red), a pair of well-defined redox peaks of $[Fe(CN)_6]^{3-/4-}$ was observed at 363 and 151 mV. The peak-to-peak separations (ΔE_p) were 525, 415, 355 and

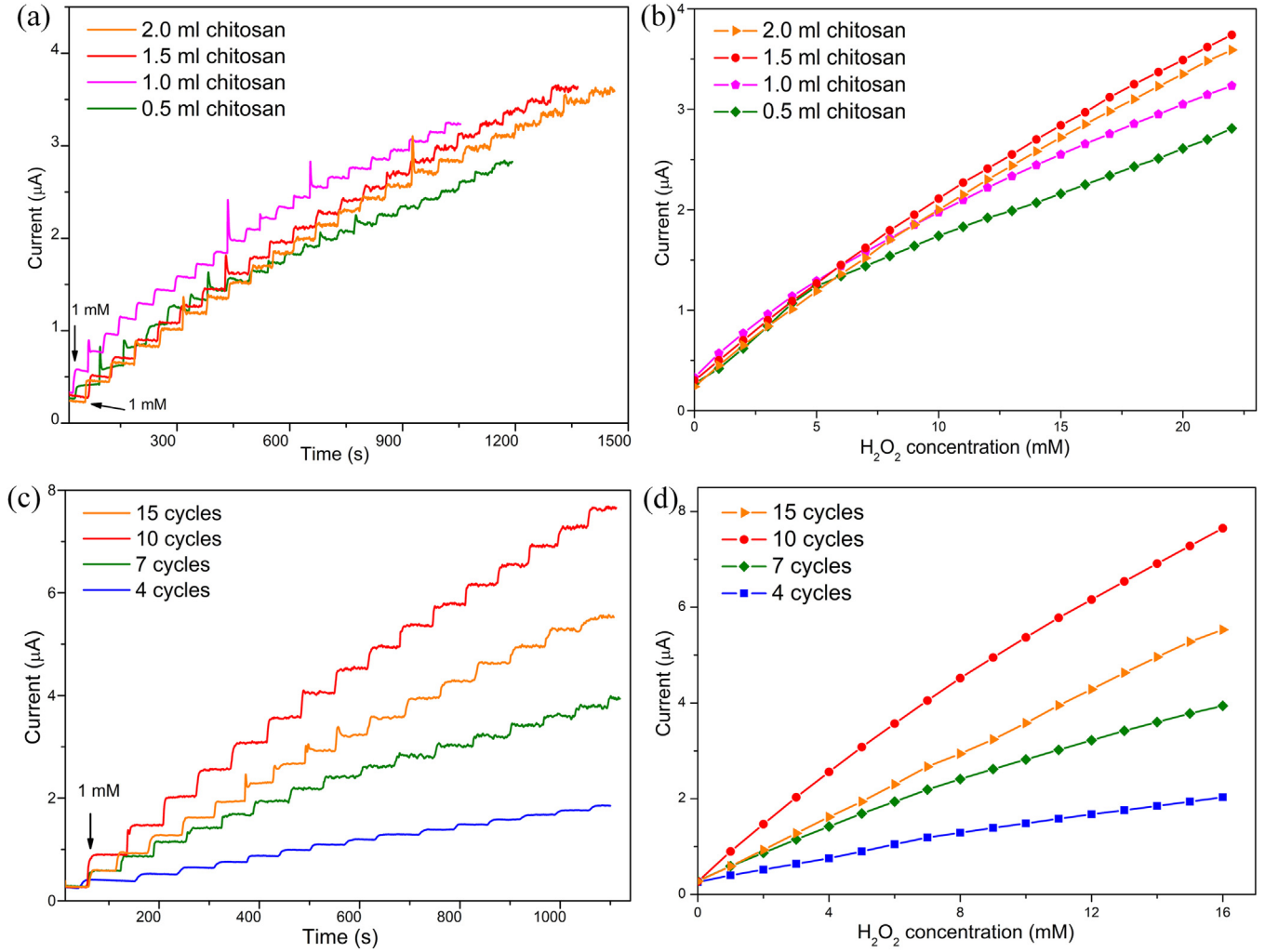

Fig. 4. Typical current-time response curve (a) and calibration curve (b) of graphene-CS/SPE for successive addition of H_2O_2 concentration with different chitosan solution volume of 0.5 mL, 1.0 mL, 1.5 mL and 2.0 mL. Typical current-time response curve (c) and calibration curve (d) of graphene-CS/SPE for successive addition of H_2O_2 concentration with different cyclic voltammetry scan cycles of 4 cycles, 7 cycles, 10 cycles and 15 cycles.

212 mV for bare SPE (in blue), graphene/SPE (in orange), CS/SPE (in green) and graphene-CS/SPE (in red), respectively, suggesting the fairly fast electron transfer at the graphene-CS/SPE. The peak current at the graphene/SPE is higher than bare SPE, which was attributed to excellent conductivity of pristine graphene although the amount of pristine graphene immobilized on the SPE was hardly realized from Fig. S4. The enhanced electron transfer at CS/SPE can be ascribed to the introduction of CS via electrodeposition. The strong electrostatic interactions between positively charged CS and negatively charged $[Fe(CN)_6]^{3-/4-}$ lead to the improved electrochemical performance at CS/SPE, which is in accordance with previous reports [19,20]. The fairly enhanced fast electron transfer at the graphene-CS/SPE is attributed to the synergistic effect between graphene and chitosan. The distinct increase in peak current for graphene-CS/SPE compared to that of CS/SPE also indicates that pristine graphene was successfully immobilized with the CS films via electrodeposition and the electrochemical performance was improved.

The electroactive surface area of electrode could be estimated according the Randles-Sevcik equation:

$$I_p = 2.69\times10^5 \times n^{3/2}ACv^{1/2}D^{1/2}$$

where I_p corresponds to the peak current, n is the number of electron participating in the reaction (n = 1), A represents the area of electrode, C relates to the concentration of the probe molecule in the solution (10 mM), v relates to the scan rate (50 mV/s) and D is the diffusion coefficient. The value of A can be calculated according the above equation. The obtained value of electroactive surface area for graphene-CS/SPE was about 1.393, 1.260 and 1.258 times larger than those of the SPE, graphene/SPE and CS/SPE respectively, attributed to the layer-by-layer structure formed at the graphene-CS/SPE. Hence, the above results clearly show that the modification of graphene-chitosan hybrid film via one-step electrodeposition method is a more adequate mediator to transfer electron and enhance electro-catalytic current.

3.3. Improvement of the detection performance of graphene-chitosan for H_2O_2

In order to explore the electrochemical sensor applications of the graphene-chitosan, enzyme-free hydrogen peroxide biosensor was fabricated. H_2O_2 was electrochemical oxidized at the surface of graphene-CS/SPE surface and the oxidation current was detected. The improved performance of graphene-CS for H_2O_2 detection was examined by the amperometric response comparision between the graphene-CS/SPE and bare SPE as displayed in Fig. 3b. The graphene-CS/SPE was carried out by CV with potential window from − 1.5–0.6 V at a scan rate of 50 mV/s for 7 cycles in 2 mL graphene and 1 mL chitosan mixed solution. Fig. 3b shows the typical current-time response for successive addition curve and Fig. 3c displays the corresponding calibration curve of H_2O_2

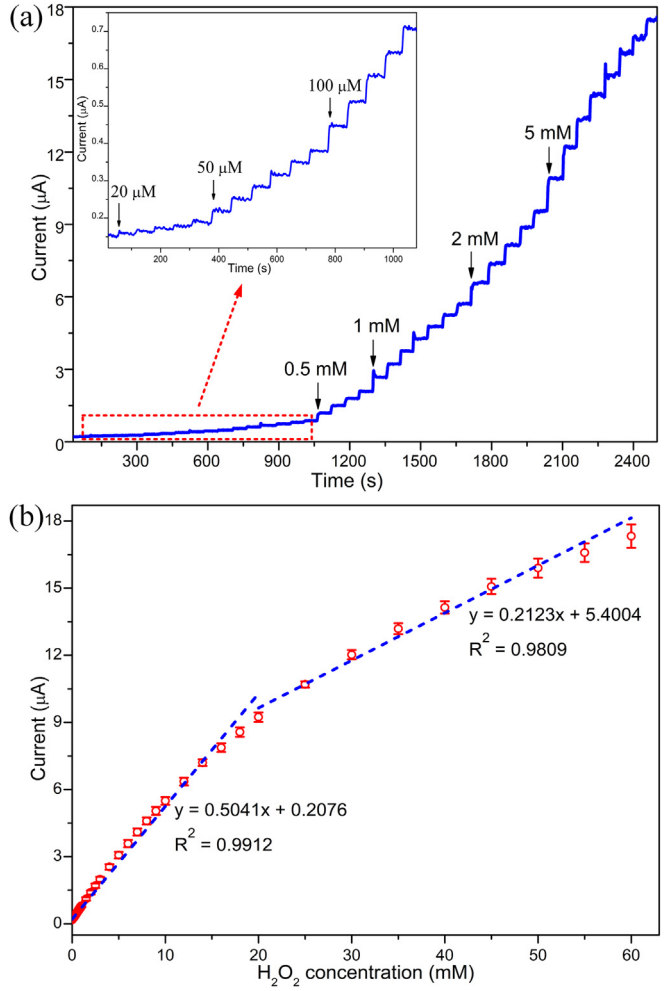

Fig. 5. (a) Typical current-time response curve of the graphene-CS/SPE for the successive injection of H_2O_2 at the applied potential of 0.6 V (vs. Ag/AgCl); the inset displays the current-time response at low H_2O_2 concentration. (b) the corresponding calibration curve for H_2O_2 detection (mean ± SD, n = 4).

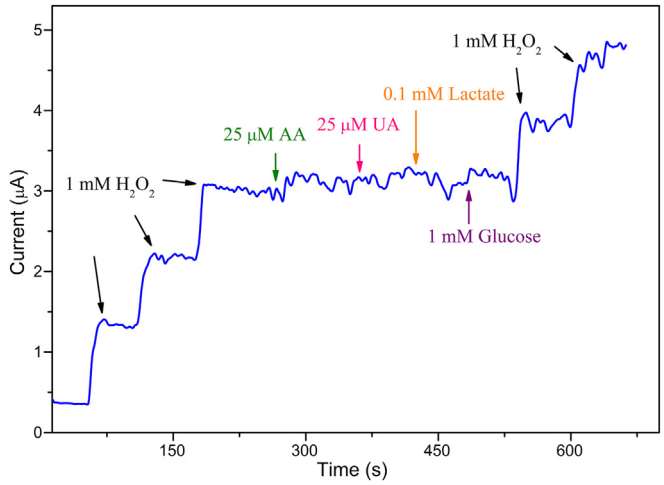

Fig. 6. Interference test of graphene-CS/SPE in 0.01 M PBS solution at an applied potential of 0.6 V with 1 mM H_2O_2, 25 μM AA, 25 μM UA, 0.1 mM lactate, 1 mM glucose.

for bare SPE (in blue) and graphene-CS/SPE (in red) at an applied potential of 0.6 V respectively. The abnormal current jumping in Fig. 3b caused by H_2O_2 addition and the response current reached equilibrium afterwards. The bare SPE showed a slow increase upon the addition of H_2O_2, with a response time more than 10 s, a sensitivity of 0.036 μA mM^{-1} cm^{-2} and a narrow range about 10 mM. The graphene-CS/SPE showed a much higher sensitivity of 1.87 μA mM^{-1} cm^{-2}, approximately 52 times larger than that of bare SPE. In addition, the graphene-CS/SPE exhibited a wider linear range up to 22 mM with a shorter response time less than 3 s. The modification of graphene-chitosan through co-electrodeposition in this work significantly improved the performance of the electrodes for H_2O_2 determination.

3.4. Optimization of the fabrication conditions of graphene-chitosan/SPE

Electroactivity of the graphene-chitosan film is largely related to the amount of graphene nanoplates co-electrodeposited with chitosan and the thickness of the graphene-CS film. Therefore, in order to obtain optimal sensitivity and linearity for H_2O_2 detection, the volume ratio of graphene nanoplates dispersion and chitosan solution and CV scan cycles during the deposition process were investigated. The abnormal current jumping in Figs. 4a and 4c caused by H_2O_2 addition and the response current reached equilibrium within 3 s. As displayed in Figs. 4a and 4b, the current response increased with increasing the volume of chitosan solution from 0.5 to 1.5 mL to achieve a maximum at 1.5 mL and remained thereafter (the volume of graphene nanoplates dispersion fixed at 2.0 mL). The phenomenon might be attributed to the fact that the electrostatic interactions between positively charged chitosan and negatively charged graphene nanoplates changed along with the different volume ratio of graphene nanoplates dispersion and chitosan solution, resulting in the different amount of graphene nanoplates encapsulated onto the electrodes during co-electrodeposition. When the volume of chitosan increased from 0.5 to 1.5 mL, the amount of graphene nanoplates encapsulated onto the electrodes increased, leading to a larger surface area, and thus the electrocatalytic activity of the graphene-CS to H_2O_2 greatly improved and an increase in current response. While chitosan increased continuously, the amount of graphene nanoplates absorbed to chitosan by electrostatic interactions was saturated and the redundant graphene nanoplates might aggregate due to strong π-π interaction, resulting in a slight decrease in the amount of graphene nanoplates encapsulated onto the electrodes, showing as a slight decrease in current response. Thus, with respect to sensitivity, the optimal graphene-chitosan solution volume ratio was 4:3 (2 mL: 1.5 mL) and used for thereafter experiments.

The effect of numbers of CV scan cycles upon H_2O_2 determination during graphene-chitosan electrodeposition process has also been evaluated as shown in Figs. 4c and 4d. The current response increased largely with increasing the number of scan cycles from 4 to 10, reached the maximum at 10 cycles and decreased thereafter. The reason of the phenomenon might be that the amount of graphene nanoplates and chitosan electrodeposited onto the electrodes increased with an increase of the number of scan cycles, enhancing the catalytic activity for H_2O_2 reduction. When the number of scan cycles increased to 15 cycles, the current response decreased, probably owing to the obtained graphene-CS film getting much more compact, hindering the solution diffusion and electron transfer. Therefore, 10 CV scan cycles were selected as the optimal electrodeposition conditions for further research.

3.5. Electrochemical performance of graphene-CS/SPE towards hydrogen peroxide

Electrocatalytic performance of the graphene-CS/SPE towards hydrogen peroxide has been investigated in Fig. 5. The typical time-current response of the graphene-CS/SPE to the successive additions of H_2O_2 in 0.01 M stirring PBS solution under the applied potential of 0.6 V was demonstrated in Fig. 5a. As can be seen, the response current increased with each injection of H_2O_2 and achieved 95% of the steady-state current in less than 3 s. The inset of Fig. 5a demonstrates the amperometric response for low H_2O_2 concentration detection.

Fig. 5b displays the corresponding calibration curve for a series of 4 electrodes (mean ± standard deviation) with good reproducibility. As can be seen, the sensor exhibited two linear dynamic ranges from 20 μM to 20 mM (R^2 = 0.9912) and 20–60 mM (R^2 = 0.9809), and the detection limit is estimated to be 5 μM at a signal-to-noise of 3. In addition, the linear equations were $i = 0.2076 + 0.5041\ C$ and $i = 5.4004 + 0.2123\ C$ (i in μA, C in mM), with the sensitivity of 6.42 μA mM^{-1} cm^{-2} and 2.86 μA mM^{-1} cm^{-2}, approximately 178 and 79 times larger than that of bare SPE respectively. The phenomenon of two linear range for H_2O_2 determination is owing to the adsorption process on the surface of graphene-CS/SPE as reported previously [34].

3.6. Stability, interference study and real sample analysis

The stability of the graphene-CS/SPE was investigated. After stored at room temperature (25 °C) for 6 days (n = 3), the modified electrode still remained 97.9% (RSD = 3.06%) of its original response to 1 mM H_2O_2, indicating that the constructed H_2O_2 sensor exhibited good stability.

The influence of common electrochemical interferents to H_2O_2 current response was also determined. Fig. 6 demonstrates the current response of H_2O_2 (1 mM) in the presence of ascorbic acid (AA) (25 μM), uric acid (UA) (25 μM), lactate (0.1 mM) and glucose (1 mM) in 0.01 M PBS at an applied potential of 0.6 V. The current increased by the addition of these interferents could be negligible. When 1 mM H_2O_2 added again, the current response still increased proportionally even with such interferents, suggesting a good anti-interference ability and a high selectivity of the proposed biosensors for H_2O_2. These may be owing to the good film forming ability of CS, preventing the interferents from the surface of the biosensors.

Real sample analysis of the fabricated graphene-CS/SPE was conducted in the diluted bovine serum. The volume ratio of bovine serum and 0.01 M PBS was 1:1. Table S2 demonstrates the values obtained from the recovery experiment. The recovery values are in the range of 85.3–109.9% with the RSD % values from 2.2 to 5.3 in the diluted bovine serum. The results indicate that the proposed graphene-CS/SPE can be used for H_2O_2 determination in real samples.

Various non-enzymatic hydrogen peroxide sensors with graphene-based metal-free electrocatalysts reported previously have been summarized in Table S3 with respect to the applied potential, linear range, detection limit and sensitivity. It can be seen that the graphene-CS/SPE exhibited extremely broader detection range than that based on other metal-free electrocatalysts, with two wide linear detection ranges from 20 μM to 20 mM and 20–60 mM respectively, showing a high reproducibility. The superior performance of the sensors may due to excellent electrocatalytic activity for hydrogen peroxide provided by high-quality pristine graphene. Moreover, the introduction of chitosan enabled the successful immobilization of pristine graphene onto electrodes through the electrostatic interaction between them. In addition, the co-electrodeposition of graphene nanoplates and chitosan resulted in the layer-by-layer structure and a high surface area.

4. Conclusions

In summary, a facile and effective route to directly immobilize negatively charged pristine graphene nanoplates on SPE was proposed and its electrochemical behaviors towards H_2O_2 were also investigated. Due to CS excellent film forming ability and positively charged property after protonation, CS was used to immobilize graphene nanoplates onto SPE. The co-electrodeposited graphene-CS hybrid film formed layer-by-layer structure and the successful immobilization was confirmed by several characterizations. The volume ratio of graphene nanoplates dispersion and chitosan solution and CV scan cycles were optimized. The synergistic effect of graphene and CS promotes electrochemical detection of H_2O_2 over wide linear range with a low limit of detection. The obtained H_2O_2 biosensor can provide promising platforms for the development of other biosensors and the strategy proposed in this work for direct immobilization of pristine graphene on electrodes could be extended for the immobilization of other nanomaterials and biomolecules.

Acknowledgements

This work was supported by the National Natural Science Foundation of China (61501400, 81501555); China Postdoctoral Science Foundation (2015M571879); Special Foundation of China Postdoctoral Science (2016T90541); and Natural Science Foundation of Zhejiang Province (LY18H180006).

Appendix A. Supporting information

Supplementary data associated with this article can be found in the online version at doi:10.1016/j.talanta.2018.07.038.

References

[1] S. Stankovich, D.A. Dikin, G.H.B. Dommett, K.M. Kohlhaas, E.J. Zimney, E.A. Stach, R.D. Piner, S.T. Nguyen, R.S. Ruoff, Nature 442 (2006) 282–286.
[2] T. Vats, S. Dutt, R. Kumar, P.F. Siril, Sci. Rep. 6 (2016) 33053.
[3] H. Chen, M.B. Müller, K.J. Gilmore, G.G. Wallace, D. Li, Adv. Mater. 20 (2008) 3557–3561.
[4] X. Yang, J. Zhu, L. Qiu, D. Li, Adv. Mater. 23 (2011) 2833–2838.
[5] W.J. Syu, H.P. Yu, C.Y. Hsu, Y.C. Rajan, Y.H. Hsu, Y.C. Chang, W.Y. Hsieh, C.H. Wang, P.S. Lai, Small 8 (2012) 2060–2069.
[6] D.J. Chen, Q.L. Zhang, J.X. Feng, K.J. Ju, A.J. Wang, J. Wei, J.J. Feng, J. Power Sources 287 (2015) 363–369.
[7] D.H. Du, P.C. Li, J.Y. Ouyang, ACS Appl. Mater. Interfaces 7 (2015) 26952–26958.
[8] Y. Chen, X.Y. Liu, S. Zhang, L.Q. Yang, M.L. Liu, Y.Y. Zhang, S.Z. Yao, Electrochim. Acta 231 (2017) 677–685.
[9] C. Mattevi, G. Eda, S. Agnoli, S. Miller, K.A. Mkhoyan, O. Celik, D. Mastrogiovanni, G. Granozzi, E. Garfunkel, M. Chhowalla, Adv. Funct. Mater. 19 (2009) 2577–2583.
[10] C. Gomez-Navarro, R.T. Weitz, A.M. Bittner, M. Scolari, A. Mews, M. Burghard, K. Kern, Nano Lett. 7 (2007) 3499–3503.
[11] Y.X. Fang, D. Zhang, Y. Guo, Y.M. Guo, Q. Chen, Sens. Actuators B-Chem. 221 (2015) 265–272.
[12] T. Yan, H.J. Zhang, D.D. Huang, S.N. Feng, M. Fujita, X.D. Gao, Nanomaterials 7 (2017) 59.
[13] A.M. Pandele, M. Ionita, L. Crica, S. Dinescu, M. Costache, H. Iovu, Carbohydr. Polym. 102 (2014) 813–820.
[14] N. Hernandez-Ibanez, L. Garcia-Cruz, V. Montiel, C.W. Foster, C.E. Banks, J. Iniesta, Biosens. Bioelectron. 77 (2016) 1168–1174.
[15] P. Gomathi, M.K. Kim, J.J. Park, D. Ragupathy, A. Rajendran, S.C. Lee, J.C. Kim, S.H. Lee, H.D. Ghim, Sens. Actuators B-Chem. 155 (2011) 897–902.
[16] S. Frindy, A. Primo, H. Ennajih, A.E. Qaiss, R. Bouhfid, M. Lahcini, E. Essassi, H. Garcia, A. El Kadib, Carbohydr. Polym. 167 (2017) 297–305.
[17] J. Luo, Y.Z. Chen, Q. Ma, R. Liu, X.Y. Liu, J. Mater. Chem. C 2 (2014) 4818–4827.
[18] J.Y. Liu, X.H. Wang, T.S. Wang, D. Li, F.N. Xi, J. Wang, E.K. Wang, ACS Appl. Mater. Interfaces 6 (2014) 19997–20002.
[19] J. Ou, Y.X. Tao, J.J. Xue, Y. Kong, J.Y. Dai, L.H. Deng, Electrochem. Commun. 57 (2015) 5–9.
[20] X.G. Gu, Y.X. Tao, Y. Pan, L.H. Deng, L.P. Bao, Y. Kong, Anal. Chem. 87 (2015) 9481–9486.
[21] A.M. Fernandes, M.H. Abdalhai, J. Ji, B.W. Xi, J. Xie, J.D. Sun, R. Noeline, B.H. Lee, X.L. Sun, Biosens. Bioelectron. 63 (2015) 399–406.
[22] F. Wu, T. Huang, Y.J. Hu, X. Yang, Q.J. Xie, J. Electroanal. Chem. 781 (2016) 296–303.
[23] J. Barton, M.B.G. Garcia, D.H. Santos, P. Fanjul-Bolado, A. Ribotti, M. McCaul, D. Diamond, P. Magni, Microchim. Acta 183 (2016) 503–517.
[24] F. Arduini, L. Micheli, D. Moscone, G. Palleschi, S. Piermarini, F. Ricci, G. Volpe, Trac-Trends Anal. Chem. 79 (2016) 114–126.
[25] M.U. Ahmed, M.M. Hossain, M. Safavieh, Y.L. Wong, I. Abd Rahman, M. Zourob, E. Tamiya, Crit. Rev. Biotechnol. 36 (2016) 495–505.
[26] P.P. Zuo, H.F. Feng, Z.Z. Xu, L.F. Zhang, Y.L. Zhang, W. Xia, W.Q. Zhang, Chem. Cent. J. 7 (2013) 39.
[27] J. Jose, M.A. Al-Harthi, M.A. AlMa'adeed, J.B. Dakua, S.K. De, J. Appl. Polym. Sci. 132 (2015) 41827.
[28] F. Emadi, A. Amini, A. Gholami, Y. Ghasemi, Sci. Rep. 7 (2017) 42258.
[29] D.Y. Pan, S. Wang, B. Zhao, M.H. Wu, H.J. Zhang, Y. Wang, Z. Jiao, Chem. Mater. 21 (2009) 3136–3142.
[30] G. Gao, D. Liu, S. Tang, C. Huang, M. He, Y. Guo, X. Sun, B. Gao, Sci. Rep. 6 (2016) 20034.
[31] P.-C. Li, G.M. Liao, S.R. Kumar, C.-M. Shih, C.-C. Yang, D.-M. Wang, S.J. Lue, Electrochim. Acta 187 (2016) 616–628.
[32] Y. Wang, X. Liao, Y. Luo, Q. Yang, G. Li, J. Mater. Sci. Technol. 31 (2015) 463–466.
[33] B. Liu, C.M. Yang, Z. Liu, C.S. Lai, Nanomaterials 7 (2017) 302.
[34] N.H. Al-Hardan, M.A.A. Hamid, R. Shamsudin, N.K. Othman, L.K. Keng, Sensors 16 (2016) 1004.